ARTICLE
Journal of Cellular Biochemistry 116:2074–2085 (2015)

Journal of Cellular Biochemistry

Undifferentiated Neuroblastoma Cells Are More Sensitive to Photogenerated Oxidative Stress Than Differentiated Cells

Chu-I Lee,[1]* Jing-Huei Perng,[2] Huang-Yo Chen,[1,3] Yi-Ren Hong,[4] and Jyh-Jye Wang[5]

[1]*Department of Medical Laboratory Science and Biotechnology, Fooyin University, Kaohsiung, Taiwan*
[2]*Department of Chemistry, National Kaohsiung Normal University, Kaohsiung, Taiwan*
[3]*Department of Biological Science, National Sun Yat-sen University, Kaohsiung, Taiwan*
[4]*Faculty of Medicine, Department of Biochemistry, Kaohsiung Medical University, Kaohsiung, Taiwan*
[5]*Department of Nutrition and Health Science, Fooyin University, Kaohsiung, Taiwan*

ABSTRACT

Neuroblastoma is one of the most aggressive cancers and has a complex form of differentiation. We hypothesized that advanced cellular differentiation may alter the susceptibility of neuroblastoma to photodynamic treatment (PDT) and confer selective survival advantage. We demonstrated that hematoporphyrin uptake by undifferentiated SH-SY5Y cells was lower than that of differentiated counterparts, yet the former were more susceptible to PDT-induced oxidative stress killing. Photogenerated reactive oxygen species (ROS) in undifferentiated cells efficiently stimulated cell cycle arrest at G2/M phase, mitochondrial apoptotic pathway activation, the sustained phosphorylation of Akt/GSK-3β and ERK. Differentiated cells with more resistance to PDT exhibited a ROS-independent and a prolonged activation of ERK. Both SH-SY5Y cells exposed to PDT exhibited ROS-independent p38 and JNK activation. These results may have important implications for neuroblastoma patients undergoing photodynamic therapy. J. Cell. Biochem. 116: 2074–2085, 2015.

KEY WORDS: Akt/GSK-3β; APOPTOSIS; DIFFERENTIATION; MAPKs; NEUROBLASTOMA; PHOTODYNAMIC THERAPY; REACTIVE OXYGEN SPECIES

INTRODUCTION

Neuroblastoma originates from the sympathetic neuroblasts of the peripheral nervous system. Neuroblastoma cells derive from pluripotent neural crest stem cells; they uniquely exhibit heterogeneous cellular differentiation and comprise multiple cell phenotypes including highly tumorigenic and multipotent cells (I-type), immature sympathoblasts cells (N-type), and cells similar to Schwannian/glial/melanoblastic precursor cells (S-type) [Rettig et al., 1987]. Retinoic acid (RA) is essential in embryonic development and the maintenance of epithelial, fibroblastic, and myelomonocytic cell growth and differentiation [Tang and Gudas, 2011]. The exposure of neuroblastoma cells to RA reduces tumor cell proliferation and induces differentiation [Seigel, 2011]. Previous studies have shown that human neuroblastoma SH-SY5Y cells obtain neuron-like phenotypes with neurite outgrowth and branches by all-trans-RA treatment [Lin et al., 2009]. All-trans-RA and 13-cis-RA are used in clinical treatment to induce neuroblastoma cell differentiation; they are also used in treating later stage childhood neuroblastoma to improve the survival rate [Matthay et al., 2009].

Photodynamic therapy consists of a sequence of photophysical processes between photosensitizers, red light (620–690 nm), and oxygen. When the photosensitizer is located in cancer cells, the $^1O_2$ (singlet oxygen) generated after irradiation will cause photodamage and lead to cell death [Verhille et al., 2010]. The reactive oxygen species (ROS) accumulation caused by photodynamic treatment (PDT) may activate multiple signaling cascades in cancer cells, and thereby determine whether cancer cells are adaptive to survival or death [Yoon et al., 2012]. Apoptosis is the main type of PDT-induced cancer cell death, and mitochondria ROS plays a critical role in PDT-induced apoptosis process [Ahn et al., 2012]. Hematoporphyrin (Hp) is a first-generation porphyrin-related photosensitizer for cancer

Conflict of interest: Nothing to declare.
Grant sponsor: National Science Council, Taiwan, R.O.C.; Grant numbers: NSC-99-2815-C-242-001-B, NSC-98-2314-B-242-001-MY2.
*Correspondence to: Dr. Chu-I Lee, Department of Medical Laboratory Science and Biotechnology, Fooyin University, 151 Jinxue Rd., Daliao Dist., Kaohsiung 83102, Taiwan.
E-mail: mt046@fy.edu.tw
Manuscript Received: 21 October 2014; Manuscript Accepted: 10 March 2015
Accepted manuscript online in Wiley Online Library (wileyonlinelibrary.com): 28 April 2015
DOI 10.1002/jcb.25165 • © 2015 Wiley Periodicals, Inc.

photodynamic treatment [Sibata et al., 2001]. Excitation of Hp under irradiation in tumor cells produces a large amount of ROS inducing mitochondrial apoptotic pathway activation [Choi et al., 2009]. In recent years, many studies have revealed that serine/threonine kinase Akt and mitogen-activated protein kinases (MAPK) are important signaling pathways induced by PDT and potentially cause cell death [Bozkulak et al., 2007; Weyergang et al., 2008]. However, the effect of these signaling proteins on the photocytotoxic mechanism in neuroblastoma is inconclusive.

Neuroblastoma causes approximately 15% of the cancer mortality rate in children [Siegel et al., 2013]. Surgery, autologous stem cell transplantation, radiation therapy, and chemotherapy are the common clinical treatments for neuroblastoma. Photodynamic therapy has been tested for the treatment of neuroblastoma in animal models, but the results were not promising enough; this may be due to the varying susceptibility of the heterogeneous neuroblastoma population to photodynamic therapy [Bergmann et al., 2008]. Previous studies of photodynamic therapy on neuroblastoma mainly focused on the single tumor cell type; its effectiveness in the management of different phenotypes following the differentiation of neuroblastoma cells, however, has yet to be investigated. This study investigated the susceptibility of undifferentiated and RA-induced differentiated neuroblastoma cells to Hp-PDT. It focuses on the precise mechanism of the photosensitive effect on potential apoptotic pathways and provides findings relevant for clinical treatment of neuroblastoma.

MATERIALS AND METHODS

CHEMICALS AND REAGENTS

Dulbecco's modified Eagle's medium/F12 (DMEM/F12) and fetal bovine serum (FBS) were purchased from GIBCOBRL (Gaithersburg, MD). The antibodies to β-actin (sc-47778), cyclin B1(sc-245), Bcl-2 (sc-7382), PARP (sc-7150), caspase-9 (sc-133109), GSK-3β (sc-7291), p-GSK-3β (sc-11757), ERK (sc-135900), p-ERK (sc-7383), p38 (sc-7972), p-p38 (sc-166182), JNK (sc-7345), and p-JNK (sc-6254) were obtained from Santa Cruz Biotechnology (Santa Cruz, CA). The Akt (#4691) and p-Akt (Ser473) mAb (#4060) were obtained from Cell Signaling Technology (Boston, MA). The annexin V-fluorescein isothiocyanate (FITC) apoptosis detection kit was purchased from Strong Biotech (Taipei, Taiwan). The ECL detection kit was purchased from Amersham Life Science (Cleveland, OH). Caspase-3 colorimetric assay kits were purchased from BioVision (Mountain View, CA). Hematoporphyrin, 2′,7′-dichlorodihydrofluorescein diacetate (H_2DCFDA), Trans-retinoic acid, rhodamine 123, *N*-acetylcysteine (NAC), SP600125, SB220025, 3-(4,5-dimethylthiazol-2-yl)-2,5-diphenyltetrazolium bromide (MTT), propidium iodide (PI), Hoechst 33258, and other chemicals were purchased from Sigma Chemical Co. (St. Louis, MO).

CELL CULTURE, CELL DIFFERENTIATION, AND CELL GROWTH RATE

Human neuroblastoma cells (SH-SY5Y; ATCC CRL-2266) were cultured in DMEM/F12 medium supplemented with 10% FBS, 1% nonessential amino acids, 100 IU/mL penicillin, and 100 mg/mL streptomycin at 37°C in a humidified 5% CO_2 incubator. Cells were used early passage P11-15 and cultured up to 70% confluence in 100-mm diameter dishes and fed once every 3 days. To induce neuronal differentiation, SH-SY5Y cells were seeded at 1×10^6 cells/cm^2 in 100-mm diameter culture dishes in DMEM/F12 medium containing 10% FBS. When cells were 40–50% confluent, differentiation was initiated by addition of 10 μM all trans-RA. The cells were kept under these conditions for 5 days, changing the medium every 2 days. Cells were analyzed under phase contrast light microscopy to evaluate differences in cell morphology of proliferative cells and cells differentiated for 5 days. For cell growth rate, cells were seeded on 60 mm culture dishes at 2×10^4 cells. At the indicated times, the total cell numbers were counted

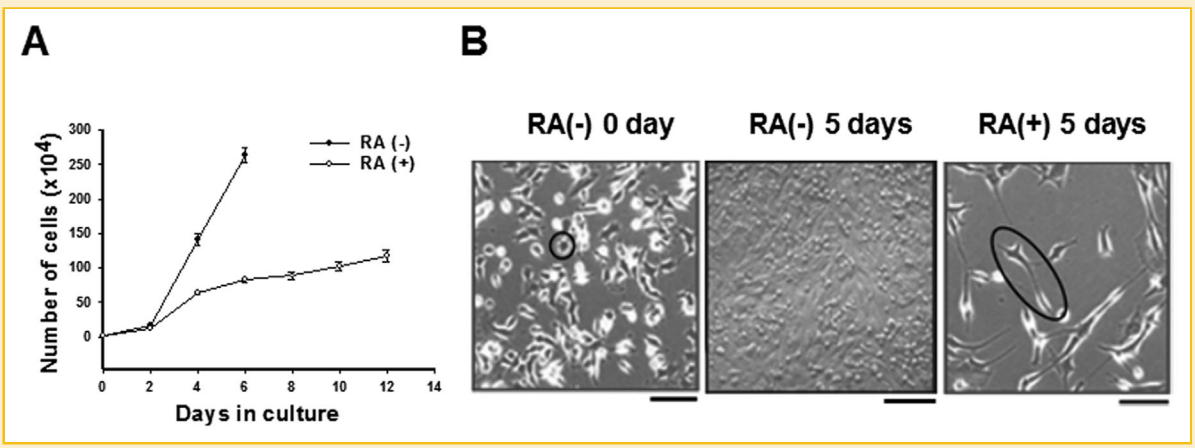

Fig. 1. Effect of RA on the growth of SH-SY5Y cells. (A) Growth rate of SH-SY5Y cells in the presence or absence of RA (10 μM). The cell number was counted by trypan blue exclusion analysis at the indicated time. Data are mean ± S.E.M. ($n = 15$). (B) Phase-contrast image of non-RA treated and RA treated SH-SY5Y cells. RA treatment induced elongation of neurites in native SH-SY5Y cells after 5 days. Scale bar, 20 μm. Circles are shown for morphological changes in non-differentiated and RA-induced differentiated SH-SY5Y cells.

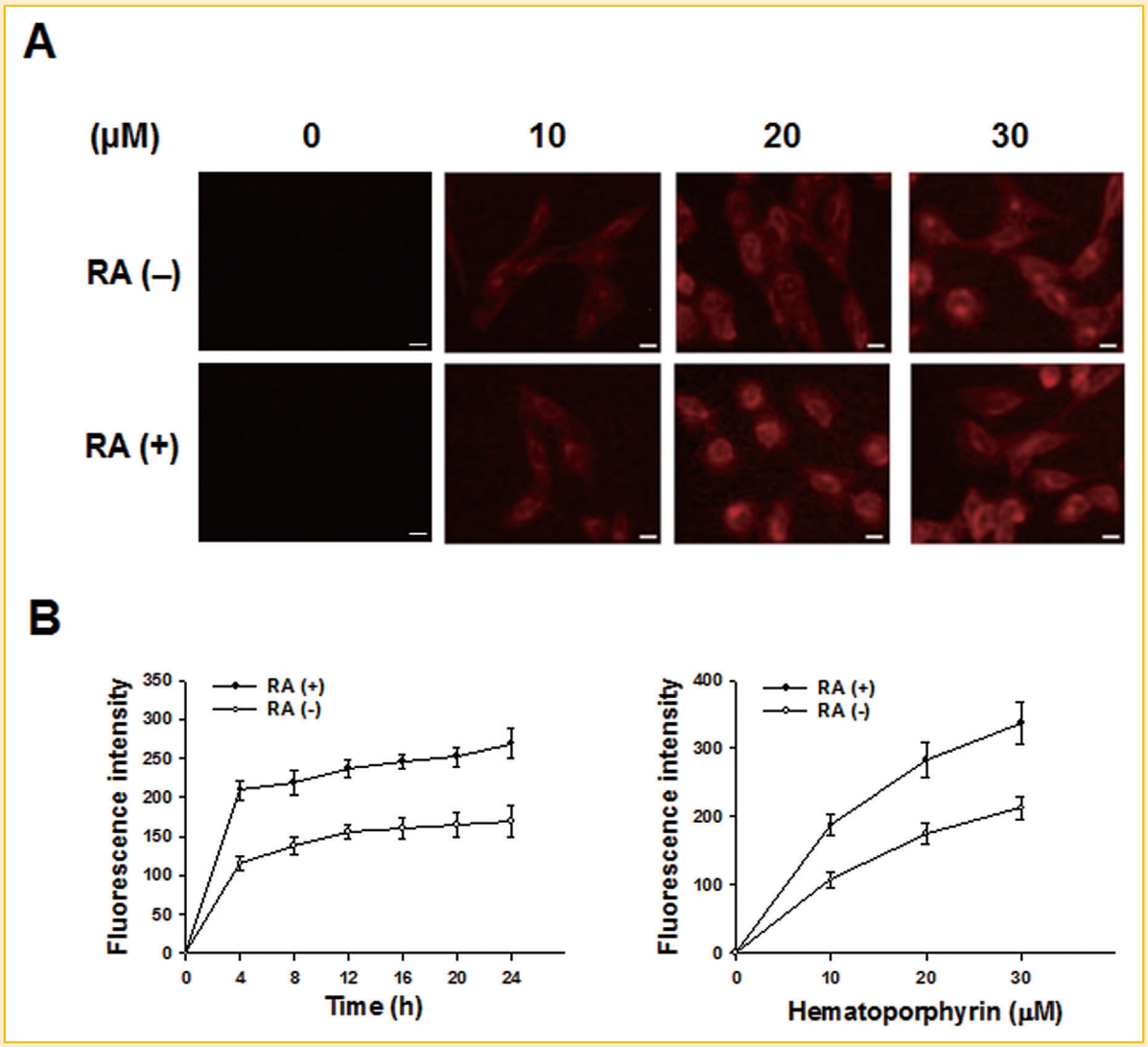

Fig. 2. Differences in Hp uptake by undifferentiated and differentiated SH-SY5Y cells. (A) Both SH-SY5Y cells were treated with different concentrations of Hp (10, 20, 30 μM) for 24 h, and the intracellular Hp fluorescence was observed using a fluorescence microscope (Bar = 10 μm). Control cells were not treated with Hp. (B) The uptake of cellular fluorescence was quantified using a flow cytometer at various incubation times (Left panel, cells were treated with 20 μM Hp) and at indicated concentrations of Hp for 24 h (Right panel). Data were normalized to RA(−) negative control cells. The vertical bars indicate the means ± S.E.M. (n = 15).

manually with a hemocytometer using the trypan blue exclusion analysis.

DRUG UPTAKE ASSAY

The cultured cells were seeded overnight in 60 mm culture dishes and incubated with a photosensitizer in the dark. Following incubation with the photosensitizer, cells were washed twice with phosphate-buffered saline (PBS) to remove any residual drug. To investigate the distribution of intracellular Hp, the cells were examined by inverted fluorescence microscope set at excitation and emission wavelengths of 405 and 632 nm, respectively. The cellular fluorescence was quantified using a FACScan flow cytometer (Becton Dickinson). Fluorescence intensity of the photosensitizer was measured by PMT4 channel after passing a 610 nm long pass filter with excitation at 488 nm. 1×10^4 events were recorded for each sample.

LIGHT IRRADIATION

The cultured cells were incubated with various concentrations of Hp for 24 h at 37°C in the dark. Subsequently, the medium containing the drug was removed, the cells were rinsed with PBS, and the medium replaced with fresh DMEM/F12. The cells were then exposed to a 625-nm LED light at a light fluence rate of 9 mW/cm^2. The controls cells were incubated with 20 μM of Hp without light irradiation for corresponding PDT experimental groups.

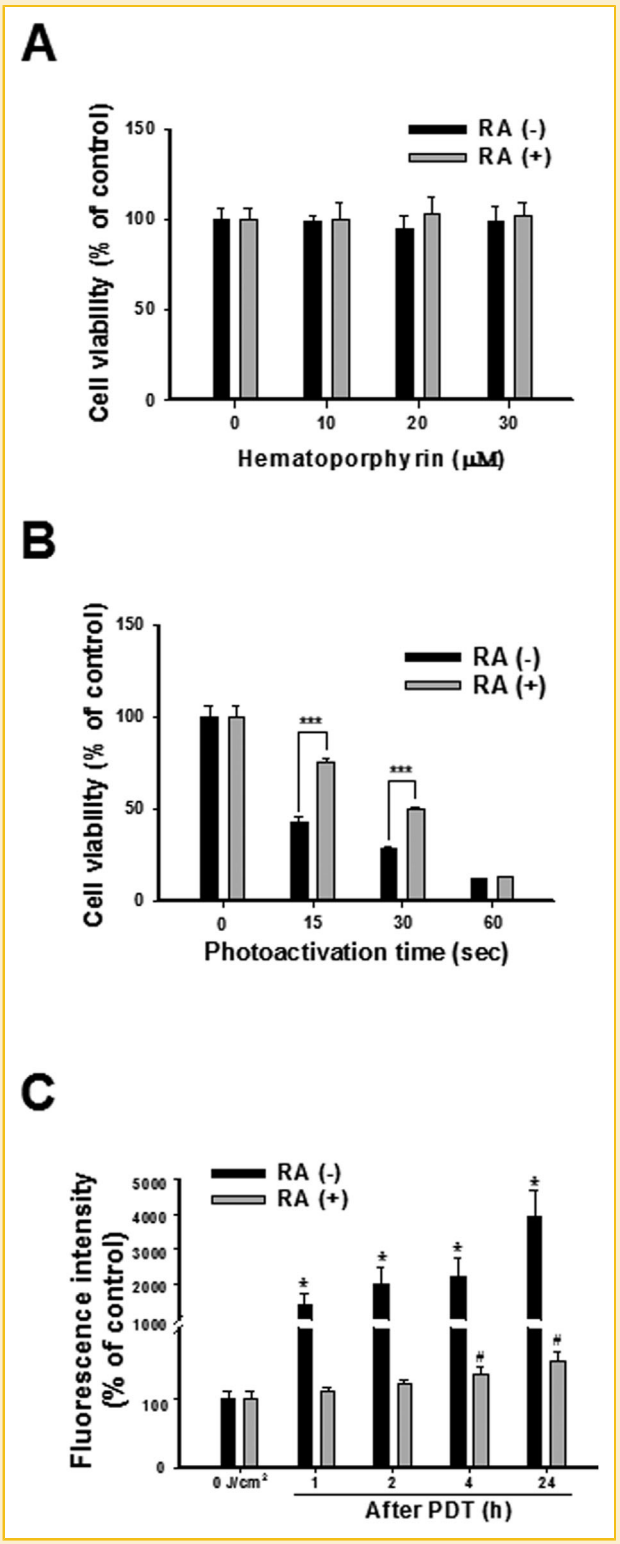

Fig. 3. Effect of Hp-PDT on the viability and ROS generation of undifferentiated and differentiated SH-SY5Y cells. (A) Cells were treated with various concentrations of Hp without irradiation and the cell viability (% of control) was assayed by MTT 24 h later. (B) Cells were treated with 20 μM Hp for 24 h, followed by photoactivation with a light fluence rate of 9 mW/cm^2 for the indicated time with MTT assay 24 h later. Data were normalized to RA(−) negative control cells. Results are presented as means ± S.E.M. ($n = 15$). $^{***}P < 0.001$ indicates significant differences between PDT-treated undifferentiated and differentiated SH-SY5Y cells. (C) Cells were treated with 20 μM Hp without irradiation as control or 15 s of Hp-PDT treatment (0.135 J/cm^2) and incubated for the indicated time. At the end of the incubation time, cells were then loaded with H_2DCFDA fluorescence, followed by flow cytometer analysis. Data were normalized to RA(−) negative control cells. Results are presented as means ± S.E.M. ($n = 15$). Significantly different from the undifferentiated control group at $^{*}P < 0.05$. Significantly different from the differentiated control group at $^{\#}P < 0.05$.

TABLE I. Cell Cycle Distribution in Undifferentiated and Differentiated SH-SY5Y Cells at 24 h Post-PDT

		Treatment		
Phase	Cells	0 J/cm^2	PDT (0.135 J/cm^2)	PDT (0.27 J/cm^2)
Sub-G1	RA (−)	0.16 ± 0.01%	10.95 ± 0.90%**	39.13 ± 2.36%**
	RA (+)	0.23 ± 0.03%	8.05 ± 0.53%$^{\#\#}$	17.68 ± 1.42%$^{\#\#}$
G0/G1	RA (−)	32.59 ± 2.43%	10.41 ± 0.26%**	15.11 ± 0.30%**
	RA (+)	33.76 ± 1.96%	35.55 ± 1.59%	31.66 ± 2.46%
S	RA (−)	50.27 ± 2.91%	46.19 ± 2.34%	33.06 ± 1.25%**
	RA (+)	51.38 ± 1.11%	42.45 ± 3.10%$^{\#}$	39.99 ± 1.65%$^{\#\#}$
G2/M	RA (−)	14.14 ± 0.87%	29.40 ± 1.85%**	11.82 ± 0.28%*
	RA (+)	11.85 ± 1.14%	12.00 ± 0.84%	10.34 ± 0.75%

Twenty-four hours after exposure to a light fluence rate of 0.135 J/cm^2 and 0.27 J/cm^2, cells were examined with PI fluorescence and analyzed by flow cytometer. Cells were treated with 20 μM Hp without irradiation as control. The data were normalized and calculated as a percentage of the control value and they represent the mean ± S.E.M. (n = 15). Significantly different from the undifferentiated control group at $^{*}P < 0.05$, $^{**}P < 0.01$. Significantly different from the differentiated control group at $^{\#}P < 0.05$, $^{\#\#}P < 0.01$.

CELL VIABILITY ASSAY

The measurement of cell viability was performed according to a previously published method [Lee et al., 2013]. Cell viability was assayed by MTT. Fifty microliters of MTT solution was added to each well (5 mg/mL in stock solution), and plates were incubated at 37°C for 2 h. The resulting formazan crystals were dissolved with DMSO (100 μL) and absorbance was read at 570 nm in an ELISA reader.

CELL CYCLE ANALYSIS

The analysis of cell cycle was performed according to a previously published method [Lee et al., 2013]. Cells were fixed with 70% ethanol at –4°C for 18 h. After washing twice with cold PBS, 3×10^6 cells were resuspended in 1 mL of staining solution [1× PBS, 1 mg/mL RNase A, 1 mg/mL PI] at room temperature for 30 min. A minimum of 10,000 cells per sample were acquired on a FACScan flow cytometer and analyzed with ModFit LT V3.0 software.

ANALYSIS OF CELL APOPTOSIS BY ANNEXIN V-FITC/PI DOUBLING STAINING

The analysis of cell apoptosis was performed according to a previously published method [Lee et al., 2013]. After treatment, cells were washed twice in PBS and resuspended in binding buffer. Cells were then stained with annexin V-FITC and PI according to the manufacturer's instructions. They were incubated in the dark at 25°C for 15 min. A minimum of 10,000 cells per sample were acquired on a FACScan flow cytometer and analyzed with CellQuest software (version 4.0.2, Becton Dickinson).

NUCLEAR STAINING WITH HOECHST 33258

Hoechst 33258 staining was applied as described previously [Lee et al., 2013]. After treatment, cells were washed twice with cold PBS, and fixed in 4% paraformaldehyde at 4°C for 30 min. The cells were then incubated in nuclear fluorochrome Hoechst 33258 at a final concentration of 5 μg/mL at room temperature for 30 min. Nuclear morphology was then examined under an inverted fluorescence microscope.

DETECTION OF INTRACELLULAR ROS GENERATION

At the end of the treatments, cells were treated with H_2DCFDA (20 μM) for 30 min in the dark at 37°C. Cells were then collected, washed, and resuspended in PBS and analyzed immediately using FACScan flow cytometry and CellQuest software (version 4.0.2, Becton Dickinson).

ASSESSMENT OF MITOCHONDRIAL MEMBRANE POTENTIAL

After treatment, cells were loaded with rhodamine 123 (10 μM) and incubated at 37°C for 30 min in the dark. Cells were then harvested, washed, and resuspended in PBS for measurement with a FACScan flow cytometer and analyzed with CellQuest software (version 4.0.2, Becton Dickinson).

COLORIMETRIC ASSAY OF CASPASE-3 ACTIVITY

Caspase activities were assessed using a colorimetric assay kit according to the manufacturer's instructions. After treatment with PDT, cells (1×10^6) were suspended in 50 μL of cell lysis buffer and incubated on ice for 10 min. Following centrifugation at 10000×*g* for 1 min, the cell lysates (50 μg) were incubated with the caspase substrate at 37°C for 1 h, and absorbance at 405 nm was measured.

WESTERN BLOTTING

Cellular lysate was prepared using lysis buffer (50 mM Tris–HCl, 150 mM NaCl, 1 mM EDTA, 1 mM EGTA, 1% Triton-X100, 20 μg/mL leupeptin, 2 mM sodium orthovanadate, 1 mM phenyl methyl sulfonyl fluoride, 5 mM sodium fluoride, and 5000 U/mL aprotinin). Equal amounts of proteins were separated on 12% SDS–PAGE and transferred onto polyvinylidene fluoride membranes. The membranes were then incubated for 2 h at room temperature with the primary antibodies. The secondary antibody was goat anti-mouse or anti-rabbit IgG conjugated to horseradish peroxidase and incubated for 1 h at room temperature. The signals were detected by an enhanced chemiluminescence detection kit.

STATISTICAL ANALYSIS

The results were expressed as the mean ± standard errors of the mean. Unpaired Student's *t*-tests were used for the comparison between two groups. One-way ANOVA analysis of variance and post hoc Tukey's test was used for comparison between more than three groups. A *P* value less than 0.05 was considered statistically significant.

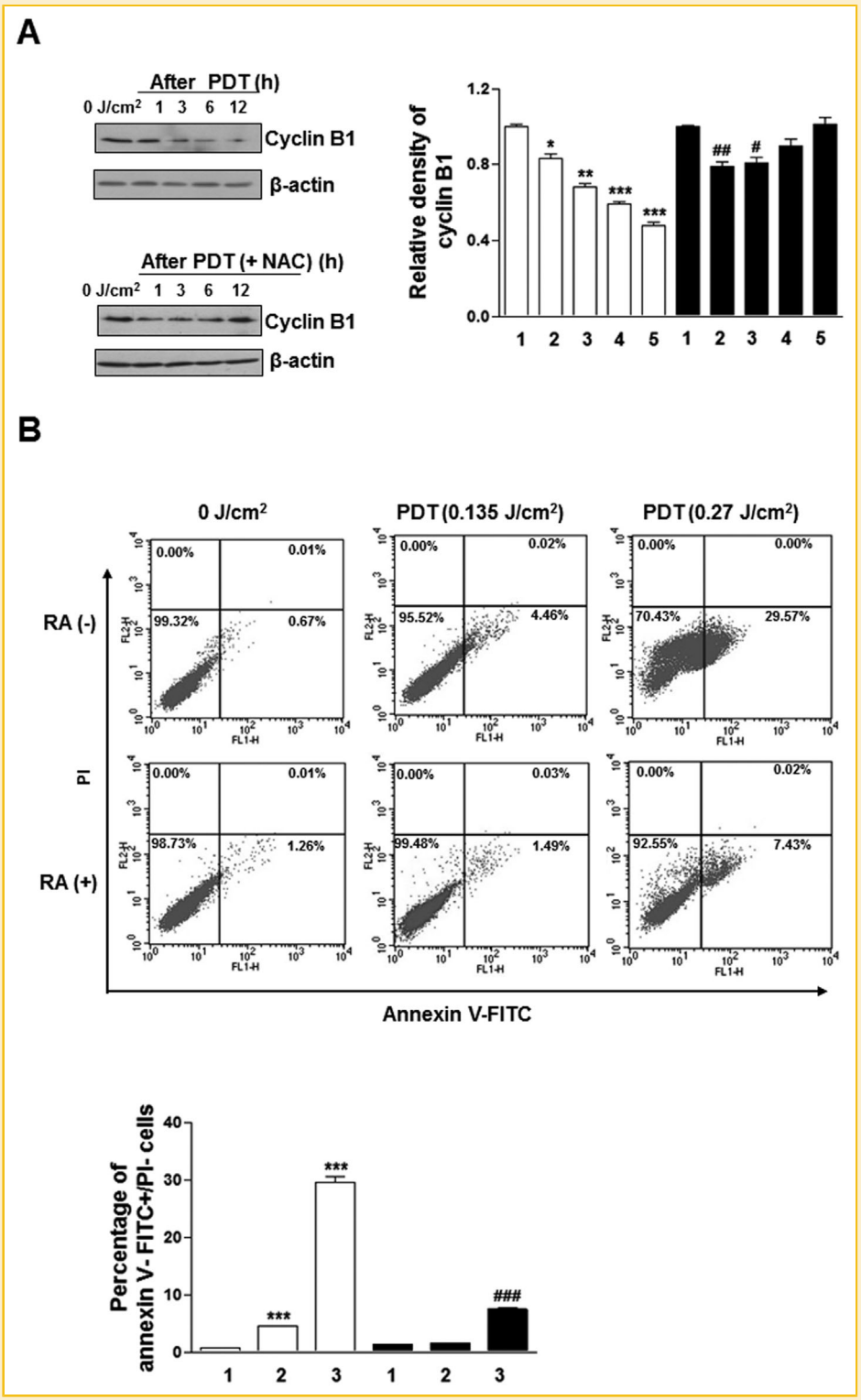

Fig. 4. Effect of Hp-PDT on cell cycle regulation and apoptotic cell percentage of undifferentiated and differentiated SH-SY5Y cells. (A) One group of undifferentiated SH-SY5Y cells was treated with 20 μM Hp for 24 h without irradiation as control (lane 1) or Hp-PDT (0.135 J/cm^2) (lanes 2–5, empty bar), and another treated with NAC (10 mM) for 1.5 h before illumination (0.135 J/cm^2) and incubated for the indicated time (lanes 1–5, closed bars). The changes in protein levels of cyclin B1 were determined by Western blot. Western blot band densitometric data obtained from duplicate determinations in 3 independent experiments are summarized and expressed as relative density change over levels of β-actin as fold control. $^{*}P < 0.05$, $^{**}P < 0.01$, $^{***}P < 0.001$, as compared with the RA(−) control. $^{\#}P < 0.05$, $^{\#\#}P < 0.01$, as compared with the RA(+) control. (B) Twenty-four hours after exposure to a light fluence rate of 0.135 J/cm^2 and 0.27 J/cm^2 (bar 2 and bar 3), cells were stained with annexin V/PI and analyzed by flow cytometry. Cells were treated with 20 μM Hp without irradiation as control (bar 1). RA(−), empty bar; RA(+), closed bars. Summaries of the apoptosis rates in histograms. $^{***}P < 0.001$, as compared with the RA(−) control. $^{\#\#\#}P < 0.001$, as compared with the RA(+) control.

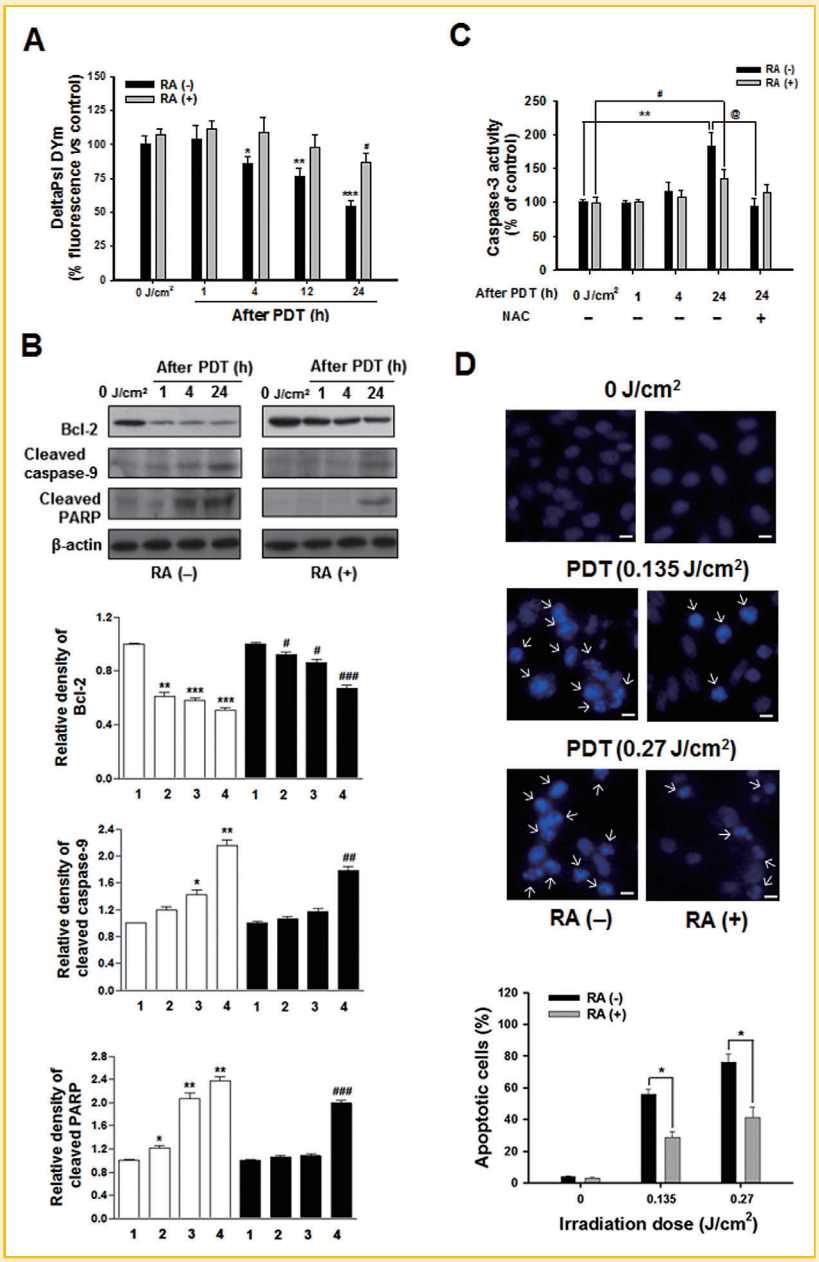

Fig. 5. The effect of Hp-PDT on apoptotic signals in undifferentiated and differentiated SH-SY5Y cells. (A) Cells were treated with Hp-PDT (0.135 J/cm^2) and incubated for the indicated time. After incubation, cells were loaded with Rhodamine123, and followed by flow cytometer analysis. Cells were treated with 20 μM Hp without irradiation as control. Data were normalized to RA(−) negative control cells. The vertical bars indicate the means ± S.E.M. (n = 15). $^{*}P < 0.05$, $^{**}P < 0.01$, $^{***}P < 0.001$, as compared with the RA(−) control. $^{\#}P < 0.05$, as compared with the RA(+) control. (B) Cells were treated with 20 μM Hp for 24 h without irradiation as control (lane 1) or Hp-PDT (0.135 J/cm^2) and incubated for the indicated time (lanes 2–4). RA(−), empty bar; RA(+), closed bars. The changes in protein levels of Bcl-2, cleaved caspase-9, and cleaved PARP were determined by Western blot. Western blot band densitometric data obtained from duplicate determinations in three independent experiments are summarized and expressed as relative density change over levels of β-actin as fold control. $^{*}P < 0.05$, $^{**}P < 0.01$, $^{***}P < 0.001$, as compared with the RA(−) control. $^{\#}P < 0.05$, $^{\#\#}P < 0.01$, $^{\#\#\#}P < 0.001$, as compared with the RA(+) control. (C) Cells were treated with 20 μM Hp without irradiation or Hp-PDT (0.135 J/cm^2) for indicated time periods by colorimetric assay. Data were normalized to RA(−) negative control cells. $^{**}P < 0.01$, indicates a significant difference between PDT-induced undifferentiated SH-SY5Y cells and the undifferentiated SH-SY5Y cell control. $^{\#}P < 0.05$, indicates a significant difference between PDT-induced differentiated SH-SY5Y cells and the differentiated SH-SY5Y cell control. $^{@}P < 0.05$ indicates a significant difference between pre-treated *N*-acetylcysteine (NAC) cells (10 mM) and the PDT control cells. (D) Cells were stained with Hoechst 33258 after Hp-PDT for 24 h, and the percentage of apoptotic cells with condensed nuclei was determined by an inverted fluorescence microscope. Scale bar, 10 μm. Uniformly stained nuclei were scored as healthy, viable nuclei while those with condensed or fragmented nuclei were identified as damaged one. Data were gathered from three separate experiments. Within each experiment, two wells per condition and at least 300 cells were counted in six randomly chosen fields per well. Quantification of the percentage of apoptotic cells corresponding to the experiments is illustrated in fluorescence micrographs. The vertical bars indicate the means ± S.E.M. $^{*}P < 0.05$ indicates a significant difference between undifferentiated SH-SY5Y cells and the differentiated SH-SY5Y cells.

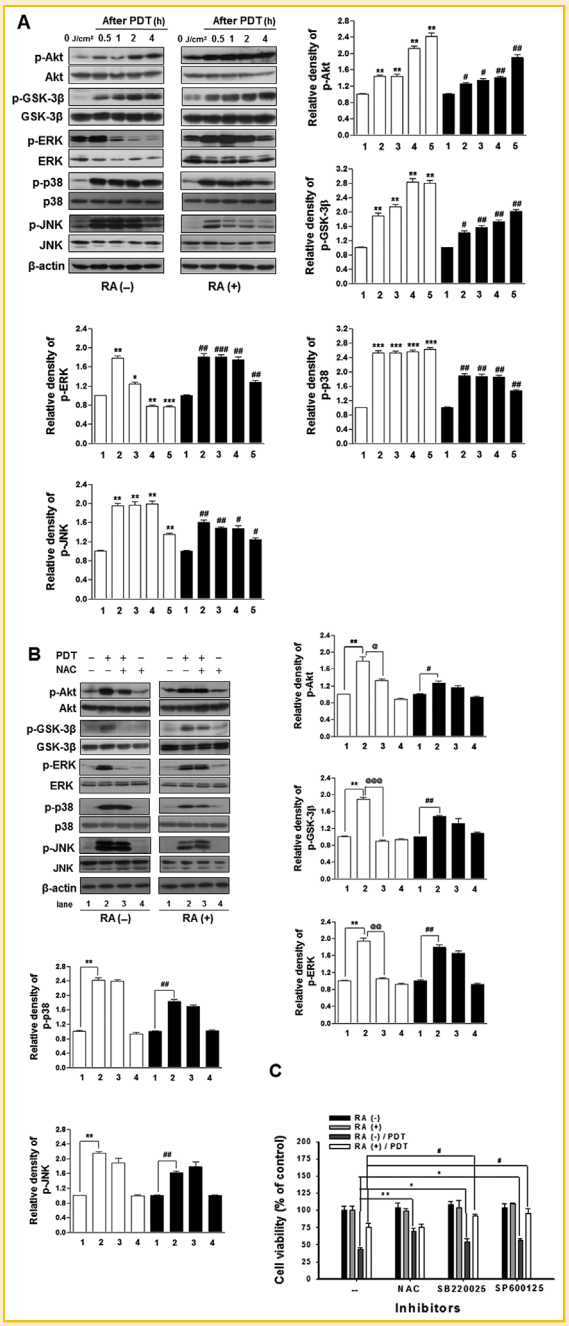

Fig. 6. The role of ROS on the activation of Akt/GSK-3β and MAPKs signaling pathways in Hp-PDT-mediated undifferentiated and RA-differentiated SH-SY5Y cells. (A) Cells were treated with 20 μM Hp for 24 h without irradiation as control (lane 1) or Hp-PDT (0.135 J/cm^2) and incubated for the indicated time (lanes 2–5). RA(−), empty bar; RA(+), closed bars. Kinetics of Akt, GSK-3β, ERK, p38, and JNK activation induced by PDT were determined by Western blot analysis. Western blot band densitometric data obtained from duplicate determinations in three independent experiments are summarized and expressed as relative density change over levels of total Akt, GSK-3β, ERK, p38, and JNK as fold-control. $^{*}P<0.05$, $^{**}P<0.01$, $^{***}P<0.001$, as compared with the RA(−) control. $^{\#}P<0.05$, $^{\#\#}P<0.01$, $^{\#\#\#}P<0.001$, as compared with the RA(+) control. (B) Cells were pre-incubated with NAC (10 mM) for 1.5 h, followed by treatment with Hp for 24 h, after which irradiation was carried out (0.135 J/cm^2) and effects of ROS scavenger on PDT-induced phosphorylation of Akt, GSK-3β, ERK, p38, and JNK were assessed at 0.5 h post-irradiation dark incubation by Western blot. RA(−) lanes 1–4, empty bars; RA(+) lanes 1–4, closed bars. Western blot band densitometric data obtained from duplicate determinations in three independent experiments are summarized and expressed as relative density change over levels of total Akt, GSK-3β, ERK, p38, and JNK as fold-control. $^{**}P<0.01$, as compared with the RA(−) control. $^{\#}P<0.05$, $^{\#\#}P<0.01$, as compared with the RA(+) control. $^{@}P<0.05$, $^{@@}P<0.01$, $^{@@@}P<0.001$, indicates a significant difference between pre-treated *N*-acetylcysteine (NAC) cells and the PDT control cells. (C) Cells were pre-incubated with NAC (10 mM), SB220025 (10 μM), or SP600125 (10 μM) for 1.5 h, followed by treatment with Hp for 24 h, after which irradiation was carried out (0.135 J/cm^2) and cell viability assessed 24 h later by MTT. Black bar, undifferentiated SH-SY5Y cells without irradiation; light gray bar, differentiated SH-SY5Y cells without irradiation; dark gray bar, undifferentiated SH-SY5Y cells after Hp-PDT; white bar, differentiated SH-SY5Y cells after Hp-PDT. Data were normalized to RA(−) negative control cells. Plotted data are means ± S.E.M. of values from three separate experiments (n = 15). $^{*}P<0.05$, $^{**}P<0.01$, $^{\#}P<0.05$ as compared with the respective control.

RESULTS

EFFECTS OF RA TREATMENT IN SH-SY5Y CELLS

A growth curve was generated in the presence or absence of RA by trypan blue exclusion analysis for the cell proliferation rate (Fig. 1A). In comparison to control cells, RA-treated SH-SY5Y cells demonstrated a quite different growth pattern, growing slowly during the first 4–12 days of treatment. RA suppressed SH-SY5Y cell growth, with 69% reduction compared to control cells after 6 days of incubation. Additionally, after 5 days of treatment with 10 μM of RA, SH-SY5Y cells exhibited morphological changes in differentiation, in which neuron-like cells were observed (Fig. 1B).

PHOTOSENSITIZER UPTAKE IN UNDIFFERENTIATED AND RA-DIFFERENTIATED SH-SY5Y CELLS

Both cells incubated with Hp for 24 h showed efficient dose-dependent cellular uptake with higher fluorescence in the RA-differentiated SH-SY5Y cells than in the undifferentiated SH-SY5Y cells by fluorescence microscope (Fig. 2A). The intracellular fluorescence intensity rate was collected in both dose- and time-dependent manner by flow cytometry analysis. Most of the uptake occurred up to 4 h followed by very slow gradual increase up to 24 h. Incubated with 20 μM Hp for 24 h, the fluorescence intensity of RA-differentiated SH-SY5Y cells was approximately 1.8 fold stronger than that of undifferentiated SH-SY5Y cells (Fig. 2B).

HP-INDUCED PHOTOCYTOTOXICITY AND ROS FORMATION IN UNDIFFERENTIATED AND RA-DIFFERENTIATED SH-SY5Y CELLS

After treating SH-SY5Y cells with different concentrations of Hp, we analyzed cell viability by MTT assay. Without irradiation, 10, 20, and 30 μM of Hp had no cytotoxicity in either group of SH-SY5Y cells (Fig. 3A). We exposed undifferentiated and RA-differentiated SH-SY5Y cells to 625-nm LED light at a light fluence rate of 9 mW/cm^2. The cytotoxic effects of PDT on both cells were time dependent. The RA-differentiated SH-SY5Y cells were significantly less sensitive to Hp-PDT than undifferentiated SH-SY5Y cells. The approximate IC_{50} of undifferentiated and RA-differentiated SH-SY5Y cells were 20 μM Hp, 15 s of irradiation (0.135 J/cm^2) and 20 μM Hp, 30 s of irradiation (0.27 J/cm^2), respectively (Fig. 3B). As shown in Figure 3C, we used H_2DCFDA-derived fluorochrome as an indicator of peroxides and superoxide accumulation in both SH-SY5Y cells. Data were normalized to RA(−) control cells. There are not any differences between RA(+) and RA(−) cells in respect to basal values for ROS. DCF fluorescence intensity significantly increased in the undifferentiated SH-SY5Y cells after Hp-PDT (0.135 J/cm^2). At 1, 2, 4, and 24 h post-irradiation dark incubation, the ROS levels of undifferentiated SH-SY5Y cells increased by 14, 19, 21, and 39 times respectively over the dark control. On the other hand, the ROS levels of RA-differentiated SH-SY5Y cells only increased by 1.1, 1.2, 1.3, and 1.5 times, respectively.

PDT-INDUCED CELL CYCLE REGULATION AND ANNEXIN V-FITC/PI APOPTOSIS IN UNDIFFERENTIATED AND RA-DIFFERENTIATED SH-SY5Y CELLS

We investigated whether Hp-PDT efficiently influenced cell cycle progression in undifferentiated and RA-differentiated SH-SY5Y cells. As shown in Table I, Hp-PDT significantly increased the population of both SH-SY5Y cells in sub-G1 phase in a dose-dependent manner. The sub-G1 population in undifferentiated SH-SY5Y cells was higher than that of the RA-differentiated SH-SY5Y cells. Moreover, under an irradiation of 0.135 J/cm^2, Hp-PDT caused undifferentiated SH-SY5Y cell arrest in G2/M phase, an effect which did not occur in RA-differentiated SH-SY5Y cells. Accordingly, we determined the expression of cyclin B1 in the Hp-PDT-induced undifferentiated SH-SY5Y cells by Western blot analysis. As shown in Figure 4A, a significant decrease in cyclin B1 levels was detected as early as 3 h after PDT. Hp-PDT-induced cyclin B1 degradation was also attenuated by treatment with ROS scavenger NAC. To further confirm the difference in Hp-PDT induced apoptosis in undifferentiated and differentiated SH-SY5Y cells, the percentage of SH-SY5Y apoptotic cells were quantified by FITC-conjugated annexin V and flow cytometric analysis. The results showed more apoptotic cells in the Hp-PDT-induced undifferentiated SH-SY5Y cell group than the differentiated SH-SY5Y cells (Fig. 4B).

PDT-INDUCED MITOCHONDRIA-MEDIATED APOPTOTIC SIGNALING PATHWAY IN UNDIFFERENTIATED AND RA-DIFFERENTIATED SH-SY5Y CELLS

We studied the effect of Hp-PDT on the mitochondrial apoptotic pathway activation in undifferentiated and RA-differentiated SH-SY5Y cells. As shown in Figure 5A, Data was normalized to RA(−) negative control cells. RA(+) control cells had a slightly higher mitochondrial membrane potential as assessed by Rhodamin123. An evident mitochondrial depolarization occurred in undifferentiated SH-SY5Y cells at 4–24 h post-PDT, but the mitochondrial membrane potential barely changed in RA-differentiated SH-SY5Y cells until 24 h post-PDT. As shown in Figure 5B, in undifferentiated SH-SY5Y cells, the expression of Bcl-2 significantly decreased at 1 h post-PDT. In RA-differentiated SH-SY5Y cells, the expression of Bcl-2 significantly decreased at 24 h post-PDT. In undifferentiated SH-SY5Y cells, Hp-PDT induced more significant caspase-9 activation than in RA-differentiated SH-SY5Y cells. The levels of cleaved poly (ADP-ribose) polymerase (PARP) in undifferentiated SH-SY5Y cells at 1, 4, and 24 h post-PDT significantly increased compared to RA-differentiated cells. As shown in Figure 5C, caspase-3 activity significantly increased at 24 h after PDT in both SH-SY5Y cells. The activity of caspase-3 at 24 h post-PDT was ∼184% and ∼135% higher than that of the non-irradiation controls of undifferentiated and RA-differentiated SH-SY5Y cells, respectively. Furthermore, the NAC significantly inhibited Hp-PDT induced caspase-3 activation in undifferentiated SH-SY5Y cells, but not in RA-differentiated SH-SY5Y cells. As shown in Figure 5D, in the absence of irradiation, SH-SY5Y cells showed nuclei with homogenous chromatin distribution. In the tested groups, dose-dependent Hp-PDT induced chromatin condensation was seen in both SH-SY5Y cells. However, the effect of chromatin condensation in undifferentiated SH-SY5Y cells was more significant than in RA-differentiated SH-SY5Y cells.

THE ROLE OF ROS ON THE ACTIVATION OF AKT/GLYCOGEN SHNTHASE KINASE-3β (GSK-3β) AND MAPK SIGNALING PATHWAYS IN PDT-MEDIATED UNDIFFERENTIATED AND RA-DIFFERENTIATED SH-SY5Y CELLS

We next investigated whether Hp-PDT would affect the intracellular signal transduction essential for stimulating cell survival and death, the Akt/GSK-3β and MAPKs signaling pathways. As shown in Figure 6A, after Hp-PDT, the expression of activated Akt and the endogenous downstream substrate GSK-3β in SH-SY5Y cells both increased. The phosphorylation of extracellular signal-regulated kinase (ERK) in RA-differentiated SH-SY5Y cells exhibited a prolonged sustained activation after Hp-PDT, whereas undifferentiated SH-SY5Y cells showed a transient activation of ERK at 0.5 h post-PDT. Concurrently, at 0.5–4 h after PDT, a marked increase in the phosphorylation of p38 and c-Jun N-terminal kinase (JNK) was observed in both cells. In addition, NAC significantly decreased Akt, GSK-3β, and ERK activation in undifferentiated SH-SY5Y cells, but not that of RA-differentiated SH-SY5Y cells. The phosphorylation of p38 and JNK was not attenuated by NAC in undifferentiated or RA-differentiated SH-SY5Y cells (Fig. 6B). Since Hp-PDT was found to induce ROS formation as well as the activation of p38 and JNK in both undifferentiated and RA-differentiated SH-SY5Y cells, specific kinase pharmacological inhibitors were used to evaluate the effect of ROS, p38, and JNK inhibition on cell viability after Hp-PDT. As shown in Figure 6C, the ROS scavenger NAC, p38 inhibitor SB220025, or JNK inhibitor SP600125 alone did not affect the viability of the cells. NAC could significantly attenuate Hp-PDT-mediated photocytotoxicity in undifferentiated SH-SY5Y cells, but not in differentiated SH-SY5Y cells. SB220025 and SP600125, however, significantly attenuated Hp-PDT-induced phototoxicity in both SH-SY5Y cells.

DISCUSSION

In this study, the differentiation of SH-SY5Y cells was characterized by an increase in their intracellular accumulation of Hp, a decrease in ROS production, and lower susceptibility to PDT. The result is in accordance with the previous studies which showed that RA-induced differentiated neuroblastoma cells have a higher resistance to apoptosis when treated with various pro-apoptotic or ROS-generating factors such as staurosporine, doxorubicin, 1-methyl-4-phenylpyridinium ion (MPP+), lactacystin, and 6-hydroxydopamine (6-OHDA) [Jantas et al., 2008; Cheung et al., 2009; Jantas et al., 2013; Jantas et al., 2014]. However, Maytin's group showed that methotrexate could promote cell differentiation and augment the efficacy of ALA-PDT for prostate cancer and skin carcinoma cell killing [Sinha et al., 2006; Anand et al., 2009]. The resistance mechanisms of differentiated SH-SY5Y cells to PDT may be multiple and complex. The physiological importance of the human ATP-binding cassette (ABC) transporter has been recognized with regard to porphyrin-mediated photosensitivity [Krishnamurthy et al., 2007]. The development of diverse tumor-targeted PDT approaches is therefore important to enhance the uptake of photosensitizers and their transport through cell membranes [Shirasu et al., 2013]. Our data suggest that differentiated cells are more mature in actively transporting Hp, so it accumulates inside the cells more than in undifferentiated ones. However, they are also more mature in ABC-transporters or changes in antioxidant capacity and endogenous antioxidant mechanisms (glutathione peroxidase, superoxide dismutase) [Erlejman and Oteiza, 2002; Golab et al., 2003; da Frota, 2011]. Additional studies are needed to determine the relationship between reduced glutathione overexpression, Cu/Zn-SOD, Mn-SOD, GPX1, CAT activities, and resistance to PDT in differentiated SH-SY5Y cells.

We investigated how the proliferation and differentiation of neuroblastoma cells were affected by ROS evolved in photosensitizing reaction. Our data showed that differentiation prevents PDT-induced apoptosis caused by mild changes of intracellular oxidative stress. Conversely, dramatic changes of oxidative stress in neuronal undifferentiated SH-SY5Y cells were observed after PDT. Several anticancer treatments (chemotherapy, radiotherapy, and photodynamic therapy) generate oxidative stress as a mechanism to cause cell death. *N*-acetylcysteine (NAC), a general antioxidant and a GSH precursor that can broadly scavenge ROS was used to reduce ROS-induced cellular stress [Lim et al., 2013]. Scavenge of ROS could significantly reverse PDT-mediated photocytotoxicity in undifferentiated SH-SY5Y cells, but not in differentiated SH-SY5Y cells. Clearly, the phototoxic effect in undifferentiated SH-SY5Y cells relies heavily on oxidative stress formation compared to differentiated SH-SY5Y cells. Notably, singlet oxygen is generally produced in the photosensitized oxidation reactions of both the above photodynamic processes in a short period of time. However, at 24 h post-irradiation dark incubation in both groups of SH-SY5Y cells, we observed dramatically different susceptibility to the oxidation of H_2DCFDA. This implied a different long-term formation of hydrogen peroxide in these cells which is known to be secondary process to PDT [Chekulayeva et al., 2006].

Many studies have shown associations between abnormal cell cycle regulation and apoptosis [Evan and Vousden 2001]. Our results illustrated that PDT exhibits a much more significant growth inhibitory effect on undifferentiated SH-SY5Y cells concomitant with the induction of cell cycle arrest and the accumulation of cells with a sub-diploid DNA content. We also demonstrated that PDT may induce change in intracellular redox status and in turn cause undifferentiated SH-SY5Y cell arrest in the G2/M phase through the degradation of cyclin B1. Therefore cell death would occur, an effect not seen in differentiated SH-SY5Y cells. These results imply ROS and cyclin B1 play an important role in the susceptibility to PDT-induced-apoptosis in undifferentiated SH-SY5Y cells.

A decrease in mitochondrial membrane potential is associated with dysfunction of mitochondria and subsequent apoptotic cell death [Chung et al., 2009]. Our data showed that the mitochondrial membrane potential dissipation caused by PDT was more significant in undifferentiated SH-SY5Y cells than that of the differentiated SH-SY5Y cells. Of note, PDT increased intracellular ROS formation concomitant with mitochondrial membrane potential loss in undifferentiated SH-SY5Y cells. These results suggest that both ROS and mitochondria play important roles in the PDT-induced apoptotic process in undifferentiated SH-SY5Y cells, and that mitochondrial ROS may be the main regulatory mechanism affected the difference in susceptibility to PDT between undifferentiated and

differentiated SH-SY5Y cells. In the present study, apart from the more significant downregulation of Bcl-2, the apoptosis induced by PDT was evidenced by more significant levels of cleaved caspase-9, cleaved PARP, and chromatin condensation in undifferentiated SH-SY5Y cells. Furthermore, we demonstrated that scavenging ROS accumulation can attenuate PDT-mediated caspase-3 activity in undifferentiated SH-SY5Y cells, but not in differentiated SH-SY5Y cells. These results suggest that apoptosis in PDT-induced undifferentiated and differentiated SH-SY5Y cells is mediated by the mitochondria/caspases pathway, and ROS is involved in the upregulation of the PDT-induced mitochondrial apoptotic pathway in undifferentiated SH-SY5Y cells.

In this study, we also investigated whether an alternative mechanism of caspase-independent apoptosis was induced by PDT in SH-SY5Y cells. Studies have shown that GSK-3β regulate different types of cell death and plays an important role in regulating the proliferation and differentiation of neuroblastoma cells [Lin et al., 2009]. However, whether GSK-3β is involved in PDT-induced cell death has yet to be reported. Our data showed that PDT resulted in sustained phosphorylation of Akt and its downstream regulatory protein GSK-3β in both SH-SY5Y cells. This result also agrees with previous reports which similarly indicate an adaptive survival mechanism of phosphorylated Akt cells in PDT-induced mouse fibroblast reactions to oxidative stress [Zhuang et al., 2003]. Previous studies have suggested that PDT would activate the two important cell death signal proteins, p38 and JNK, in the MAPKs pathway. However, ERK activation would be inhibited or only transiently phosphorylated in different types of cancer cells, and has been suggested to be proapoptotic in cells undergoing apoptosis [Tong et al., 2002; Weyergang et al., 2008]. By demonstrating that PDT induced the sustained activation of ERK, the present study accords with Tong's research in 2002. It is worth noting that prolonged ERK activation in differentiated SH-SY5Y cells may be important for cell resistance to apoptosis after PDT. We demonstrated that the level of pro-survival proteins (Bcl-2, p-Akt, and p-GSK-3β) is higher in RA-differentiated control cells than that of the undifferentiated control cells which consequently makes RA-differentiated cells more resistant to PDT. So hypothetically, a lower increase in p-Akt and p-GSK-3β after PDT in RA-differentiated cells when compared to control cells could be explained by the fact that the basal system is primed by retinoic acid. Moreover, the results suggested that ROS could only mediate PDT-induced sustained activation of Akt/GSK-3β and ERK in the proapoptotic stage and protect undifferentiated SH-SY5Y cells from death, and which did not occur in differentiated SH-SY5Y cells. ROS could only mediate PDT-induced sustained activation of Akt/GSK-3β which has been suggested to be an adaptive survival mechanism of phosphorylated Akt/GSK-3β in PDT-induced undifferentiated cells reactions to oxidative stress, and transient activation of ERK which has been suggested to be proapoptotic in cells undergoing apoptosis. Both SH-SY5Y cells exposed to PDT exhibited ROS-independent p38 and JNK activation. The decrease in PDT-mediated toxicity by p38 and JNK inhibitor indicated that activated p38 and JNK served as lethal signals in both SH-SY5Y cells after Hp-PDT. Further investigations are required to find the precise role of these signaling pathways in regulating PDT-mediated apoptosis and the relationship between the upstream mediators and downstream transcription factors. Note that the activation of Akt/GSK-3β and MAPKs signaling pathways, as well as the photogenerated ROS-induced cell cycle arrest at G2/M phase and mitochondrial apoptotic pathway activation in undifferentiated cells may all be important factors in the process of cell susceptibility to apoptosis after PDT.

Human neuroblastomas are categorized clinically by their age at diagnosis, location, metastasis, and degree of cellular maturation and heterogeneity. A high tumor cell differentiation stage correlates to favorable clinical stage and positive clinical outcome [Mohlin et al., 2011]. Most current research on human neuroblastoma is focused on the molecular and cellular analysis of the entire tumor mass. Therefore, novel strategies targeting the cellular heterogeneity of human neuroblastoma is an important requirement for the development of more effective photodynamic therapy. Phototherapy could be a first procedure to reduce the number of cancerous cells, mainly the undifferentiated and more proliferative ones. Conventional chemotherapy could be a following treatment against the surviving cells. In addition, understanding the role of ROS in the regulation network associated with susceptibility to photodynamic stress in these two cell groups with different PDT susceptibility may suggest ways to modulate the PDT effects at the molecular level and potentiate its anticancer effectiveness for this often fatal disease.

ACKNOWLEDGMENTS

This work was supported by research grants NSC-99-2815-C-242-001-B and NSC-98-2314-B-242-001-MY2 from the National Science Council, Taiwan, R.O.C. The authors are also thankful to Ms. Carol Perng for her assistance in wording improvement of the manuscript.

REFERENCES

Ahn MY, Kwon SM, Kim YC, Ahn SG, Yoon JH. 2012. Pheophorbide a-mediated photodynamic therapy induces apoptotic cell death in murine oral squamous cell carcinoma in vitro and in vivo. Oncol Rep 27:1772–1778.

Anand S, Honari G, Hasan T, Elson P, Maytin EV. 2009. Low-dose methotrexate enhances aminolevulinate-based photodynamic therapy in skin carcinoma cells in vitro and in vivo. Clin Cancer Res 15:3333–3343.

Bergmann F, Stepp H, Metzger R, Rolle U, Johansson A, Till H. 2008. In vitro and in vivo evaluation of photodynamic techniques for the experimental treatment of human hepatoblastoma and neuroblastoma: Preliminary results. Pediatr Surg Int 24:1331–1333.

Bozkulak O, Wong S, Luna M, Ferrario A, Rucker N, Gulsoy M, Gomer CJ. 2007. Multiple components of photodynamic therapy can phosphorylate Akt. Photochem Photobiol 83:1029–1033.

Chekulayeva LV, Shevchuk IN, Chekulayev VA, Ilmarinen K. 2006. Hydrogen peroxide, superoxide, and hydroxyl radicals are involved in the phototoxic action of hematoporphyrin derivative against tumor cells. J Environ Pathol Toxicol Oncol 25:51–77.

Cheung YT, Lau WK, Yu MS, Lai CS, Yeung SC, So KF, Chang RC. 2009. Effects of all-trans-retinoic acid on human SH-SY5Y neuroblastoma as in vitro model in neurotoxicity research. Neurotoxicology 30:127–135.

Choi H, Lim W, Kim JE, Kim I, Jeong J, Ko Y, Song J, You S, Kim D, Kim M, Kim BK, Kim O. 2009. Cell death and intracellular distribution of hematoporphyrin in a KB cell line. Photomed Laser Surg 27:453–460.

Chung PS, He P, Shin JI, Hwang HJ, Lee SJ, Ahn JC. 2009. Photodynamic therapy with 9-hydroxypheophorbide alpha on AMC-HN-3 human head and neck cancer cells: Induction of apoptosis via photoactivation of mitochondria and endoplasmic reticulum. Cancer Biol Ther 8:1343–1351.

Erlejman AG, Oteiza PI. 2002. The oxidant defense system in human neuroblastoma IMR-32 cells predifferentiation and postdifferentiation to neuronal phenotypes. Neurochem Res 27:1499–1506.

Evan GI, Vousden KH. 2001. Proliferation, cell cycle and apoptosis in cancer. Nature 411:342–348.

da Frota Junior ML, Pires AS, Zeidán-Chuliá F, Bristot IJ, Lopes FM, de Bittencourt Pasquali MA, Zanotto-Filho A, Behr GA, Klamt F, Gelain DP, Moreira JC. 2011. In vitro optimization of retinoic acid-induced neuritogenesis and TH endogenous expression in human SH-SY5Y neuroblastoma cells by the antioxidant Trolox. Mol Cell Biochem 358:325–334.

Golab J, Nowis D, Skrzycki M, Czeczot H, Baranczyk-Kuzma A, Wilczynski GM, Makowski M, Mroz P, Kozar K, Kaminski R, Jalili A, Kopec′ M, Grzela T, Jakobisiak M. 2003. Antitumor effects of photodynamic therapy are potentiated by 2-methoxyestradiol. A superoxide dismutase inhibitor. J Biol Chem 278:407–414.

Jantas D, Greda A, Golda S, Korostynski M, Grygier B, Roman A, Pilc A, Lason W. 2014. Neuroprotective effects of metabotropic glutamate receptor group II and III activators against MPP(+)-induced cell death in human neuroblastoma SH-SY5Y cells: The impact of cell differentiation state. Neuropharmacology 83:36–53.

Jantas D, Pytel M, Mozrzymas JW, Leskiewicz M, Regulska M, Antkiewicz-Michaluk L, Lason W. 2008. The attenuating effect of memantine on staurosporine-, salsolinol- and doxorubicin-induced apoptosis in human neuroblastoma SH-SY5Y cells. Neurochem Int 52:864–877.

Jantas D, Roman A, Kuśmierczyk J, Lorenc-Koci E, Konieczny J, Lenda T, Lasoń W. 2013. The extent of neurodegeneration and neuroprotection in two chemical in vitro models related to Parkinson's disease is critically dependent on cell culture conditions. Neurotox Res 24:41–54.

Krishnamurthy P, Xie T, Schuetz JD. 2007. The role of transporters in cellular heme and porphyrin homeostasis. Pharmacol Ther 114:345–358.

Lee CI, Lee CL, Hwang JF, Lee YH, Wang JJ. 2013. Monascus-fermented red mold rice exhibits cytotoxic effect and induces apoptosis on human breast cancer cells. Appl Microbiol Biotechnol 97:1269–1278.

Lim EJ, Oak CH, Heo J, Kim YH. 2013. Methylene blue-mediated photodynamic therapy enhances apoptosis in lung cancer cells. Oncol Rep 30:856–862.

Lin CC, Chou CH, Howng SL, Hsu CY, Hwang CC, Wang C, Hsu CM, Hong YR. 2009. GSKIP, an inhibitor of GSK3beta, mediates the N-cadherin/beta-catenin pool in the differentiation of SH-SY5Y cells. J Cell Biochem 108:1325–1336.

Matthay KK, Reynolds CP, Seeger RC, Shimada H, Adkins ES, Haas-Kogan D, Gerbing RB, London WB, Villablanca JG. 2009. Long-term results for children with high-risk neuroblastoma treated on a randomized trial of myeloablative therapy followed by 13-cis-retinoic acid: a children′s oncology group study. J Clin Oncol 27:1007–1013.

Mohlin SA, Wigerup C, Pahlman S. 2011. Neuroblastoma aggressiveness in relation to sympathetic neuronal differentiation stage. Semin Cancer Biol 21:276–282.

Rettig WJ, Spengler BA, Chesa PG, Old LJ, Biedler JL. 1987. Coordinate changes in neuronal phenotype and surface antigen expression in human neuroblastoma cell variants. Cancer Res 47:1383–1389.

Seigel GM. 2011. Differentiation potential of human retinoblastoma cells. Curr Pharm Biotechnol 12:213–216.

Shirasu N, Nam SO, Kuroki M. 2013. Tumor-targeted photodynamic therapy. Anticancer Res 33:2823–2831.

Sibata CH, Colussi VC, Oleinick NL, Kinsella TJ. 2001. Photodynamic therapy in oncology. Expert Opin Pharmacother 2:917–927.

Siegel R, Naishadham D, Jemal A. 2013. Cancer statistics, 2013. CA Cancer J Clin 63:11–30.

Sinha AK, Anand S, Ortel BJ, Chang Y, Mai Z, Hasan T, Maytin EV. 2006. Methotrexate used in combination with aminolaevulinic acid for photodynamic killing of prostate cancer cells. Br J Cancer 95:485–495.

Tang XH, Gudas LJ. 2011. Retinoids, retinoic acid receptors, and cancer. Annu Rev Pathol 6:345–364.

Tong Z, Singh G, Rainbow AJ. 2002. Sustained activation of the extracellular signal-regulated kinase pathway protects cells from photofrin-mediated photodynamic therapy. Cancer Res 62:5528–5535.

Verhille M, Couleaud P, Vanderesse R, Brault D, Barberi-Heyob M, Frochot C. 2010. Modulation of photosensitization processes for an improved targeted photodynamic therapy. Curr Med Chem 17:3925–3943.

Weyergang A, Kaalhus O, Berg K. 2008. Photodynamic therapy with an endocytically located photosensitizer cause a rapid activation of the mitogen-activated protein kinases extracellular signal-regulated kinase, p38, and c-Jun NH2 terminal kinase with opposing effects on cell survival. Mol Cancer Ther 7:1740–1750.

Yoon JH, Yoon HE, Kim O, Kim SK, Ahn SG, Kang KW. 2012. The enhanced anti-cancer effect of hexenyl ester of 5-aminolaevulinic acid photodynamic therapy in adriamycin-resistant compared to non-resistant breast cancer cells. Lasers Surg Med 44:76–86.

Zhuang S, Kochevar IE. 2003. Singlet oxygen-induced activation of Akt/protein kinase B is independent of growth factor receptors. Photochem Photobiol 78:361–371.